Photodetachment of Hydrated Sulfate Doubly Charged Anions: $SO_4^{2-}(H_2O)_n$ ($n = 4-40$)†

Xin Yang, Xue-Bin Wang, and Lai-Sheng Wang*

Department of Physics, Washington State University, 2710 University Drive, Richland, Washington 99352, and W. R. Wiley Environmental Molecular Sciences Laboratory, Pacific Northwest National Laboratory, MS K8−88, P.O. Box, Richland, Washington 99352

Received: December 20, 2001; In Final Form: January 24, 2002

We produced hydrated clusters of the sulfate dianion, $SO_4^{2-}(H_2O)_n$ ($n = 4-40$), using electrospray ionization and investigated their energetics and stabilities using photodetachment photoelectron spectroscopy (PES) at four photon energies. The adiabatic electron detachment energies of the hydrated cluster dianions were observed to increase with the number of water, from ~0.4 eV for $n = 3$, the smallest number of water to stabilize SO_4^{2-} in the gas phase, to ~5.7 eV for $n = 40$. The PES features of the smaller clusters are similar, all due to the SO_4^{2-} dianion, which was found to be in the center of the solvated clusters. The intensity of the SO_4^{2-} solute PES features was observed to decrease with solvent coverage beyond the first solvation shell ($n \approx 12$), whereas a strong high binding energy feature due to ionization of the solvent emerged. For $n > 30$, the solute PES features almost completely disappeared, and the water feature became dominant. The photon energy dependent studies allowed us to examine the repulsive Coulomb barrier (RCB), which was observed to decrease as the size of the solvated clusters increased. The RCB was also evaluated using a simple electrostatic model taking into account of both Coulomb repulsion and polarization interactions between the departing electron and the remaining singly charged solvated cluster. The RCB for ionization of water was observed to be systematically smaller than that of the solute SO_4^{2-}. The trapping of the solute photoelectrons by the solvent and the lowering of the RCB for the solvent ionization channel both contributed to the observed spectral evolution from dominance of the solute at small n to the dominance of the solvent at large n. Extrapolation of the adiabatic detachment energies of SO_4^{2-} and the ionization thresholds of water in the solvated $SO_4^{2-}(H_2O)_n$ clusters yielded bulk ionization potentials for aqueous SO_4^{2-} and water to be 12.3 and 10.05 eV, respectively.

1. Introduction

Multiply charged anions (MCAs) are ubiquitous in the condensed phase, but are rare in the gas phase.[1−6] Many familiar inorganic MCAs are not stable as isolated species because of the strong intramolecular Coulomb repulsion among the excess charges, whereas they are stabilized in the condensed phase by solvation in solution or counterions in solid. Thus, it would be of fundamental chemical and physical significance to understand how these MCAs are stabilized in the gas phase by solvent. Furthermore, such investigations provide a rare opportunity to probe the solute−solvent interactions for a class of important anions.[7−9] Understanding the properties of aqueous electrolyte solutions at a molecular level has been the focus of intensive research lately.[10−15] Singly charged cations, due to their small sizes and strong solute−water interactions, often exhibit definite solvation shells both in aqueous solutions[11,16−18] and in water clusters.[19−22] Substantial progress has recently been made in studying the solvation of multiply charged cations.[23−26] However, the solvation of anions is more complicated and microscopic information about their solvation is relatively limited, despite their importance in chemistry and biochemistry.[27−30] Most of the current research efforts on solvated anion clusters have been devoted to the simple halide anions,[31−39] with few efforts on more complex anions.[40−42] The delicate balance between water−anion and water−water interactions determines the structure of hydrated anions, which can exhibit either "surface" or "interior" state, depending on the size of the anions and the strength of the anion−water interactions.[15,34,36,38,39] MCAs are common in aqueous solutions and biomolecules and constitute a vital class of complex anions.[2−6] But there has been relatively very little experimental and theoretical effort to elucidate their stability and solvation at a molecular level.[7−9,43−46]

Photoelectron spectroscopy (PES) is a powerful technique to probe the energetics and dynamics of solvated anions. We have recently developed an experimental technique to probe gaseous MCAs using PES and an electrospray ionization (ESI) source.[6,47] The ESI technique is not only ideal to generate gaseous MCAs from solution samples,[48,49] but is also uniquely suitable for producing solvated MCAs,[7−9,43] in particular, for those MCAs that are not stable as isolated species. We have been interested in the issue of how MCAs are stabilized in the gas-phase either by counterions[50] or by solvation[7] and have mainly focused on the SO_4^{2-} dianion,[8,9,51,52] arguably one of the most common inorganic MCAs. We were able to produce hydrated sulfate clusters for a broad size range and investigated them carefully using PES. A brief account on our investigation of the stability, structures and energetics of small hydrated sulfate dianion clusters, $SO_4^{2-}(H_2O)_n$ ($n = 3-13$), have been reported.[8] We showed definitively that SO_4^{2-} requires at least

† Part of the special issue "G. Wilse Robinson Festschrift."

* To whom correspondence should be addressed. E-mail: ls.wang@pnl.gov.

10.1021/jp014632z CCC: $22.00
Published on Web 03/06/2002

three waters in the gas phase to be stabilized. We have recently reported observation of the transition from molecular behavior to bulklike features for large hydrated clusters involving both sulfate and oxalate ($C_2O_4^{2-}$).[9]

In the current paper, we report the details of our experiment and provide a full account of our investigation of the hydrated sulfate clusters, $SO_4^{2-}(H_2O)_n$ ($n = 4-40$), at four photon energies: 355, 266, 193, and 157 nm. The photon energy dependent studies allowed us to probe the repulsive Coulomb barrier (RCB), one of the most important characteristics of MCAs.[6,53-56] We observed that the RCB, which cut off high binding energy features in PES spectra, decreased as n increased. We also calculated the RCB in the hydrated sulfate clusters using a simple electrostatic model and observed good agreement with the experimentally obtained RCB as a function of cluster size. We showed that the SO_4^{2-} dianion is solvated in the center of the hydrated clusters. PES features were dominated by photoemission from the solute dianion chromophore in the small clusters. As the solvent number increased, we observed that PES features from the solute diminished as a result of increased solvent coverage and additional features from ionization of the solvent emerged. The RCB for the ionization of water was found to be consistently smaller than that of the solute, which is the charge carrier. The smaller RCB for the solvent ionization channel, along with the solvent trapping of photoelectrons from the centrally located solute, was attributed to the observed disappearance of solute PES features and the dominance of photoemission from the solvent in the large clusters.

2. Experimental Method

The experiment was carried out with a PES apparatus equipped with a magnetic-bottle time-of-flight photoelectron analyzer and an ESI source. Details of the experimental method have been given elsewhere.[47] Briefly, the $SO_4^{2-}(H_2O)_n$ clusters were produced from electrospray of a 10^{-3} M tetra-butylammonium sulfate solution in a water/acetonitrile (15/85 volume ratio) mixed solvent at neutral pH. Anions produced from the ESI source were accumulated in an ion-trap for 0.1 s before being analyzed by a time-of-flight mass spectrometer. Optimal humidity and careful control of collision-induced dissociation in the ESI source were critical for producing the hydrated sulfate clusters.

During the PES experiment, a cluster of interest was selected and decelerated before being intercepted by a probe laser beam in the photodetachment zone of the magnetic-bottle photoelectron analyzer. As we have shown previously,[6,54-56] various photon energies are critical in PES of MCAs due to the RCB. In the current study, we employed four detachment photon energies, 157 nm (7.866 eV) and 193 nm (6.424 eV) from an excimer laser, and 266 nm (4.661 eV) and 355 nm (3.496 eV) from a Nd:YAG laser. All experiments were performed at 20 Hz repetition rate with the ion beam off at alternating laser shots for background subtraction, which was critical for high photon energy experiments (>4.661 eV) due to severe background noises. Photoelectrons were collected at nearly 100% efficiency by the magnetic-bottle and analyzed in a 4-meter long electron flight tube. Photoelectron time-of-flight spectra were collected and then converted to kinetic energy spectra, calibrated by the known spectra of I^- and O^-. The electron binding energy spectra presented here were obtained by subtracting the kinetic energy spectra from the detachment photon energies. The resolution of our apparatus was about 2% ($\Delta E/E$), i.e., about 20 meV for 1 eV electrons at full anion deceleration.[47]

3. Results

3.1. Mass Spectra. Typical mass spectra of $SO_4^{2-}(H_2O)_n$ from our ESI source are shown in Figure 1. Due to the mass bias of our mass spectrometer, we can only optimize the mass signals for a limited mass range. Figure 1 shows four separately optimized mass spectra, covering the full mass range of interest currently. Hydrated sulfate dianion clusters with up to 60 water molecules were readily produced. In general, we observed monotonically decreasing mass intensities as n increased in the large cluster size range. $SO_4^{2-}(H_2O)_{36}$ appeared to be an exception (Figure 1d) and its intensity seemed to be higher than its neighbors. This may suggest a particularly stable solvation structure for the $n = 36$ cluster. However, as will be seen below, its PES spectrum is not unusual relative to that of its neighbors. The smallest cluster that we were able to observe is $SO_4^{2-}(H_2O)_3$ (Figure 1a), though the intensity of this cluster was very weak and extremely sensitive to source conditions. We never detected any smaller clusters with $n < 3$. The dominant mass peak was HSO_4^- (out of scale in Figure 1a). Interestingly, we also observed SO_4^-, which should come from autodetachment of SO_4^{2-} in the source. The mass spectra suggested that SO_4^{2-} needed at least three H_2O molecules to be stabilized in the gas phase, which was supported and confirmed by our PES results and theoretical calculations previously.[8]

3.2. PES at 355 nm. As we showed previously,[8] it was difficult to obtain the PES spectrum of $SO_4^{2-}(H_2O)_3$ due to its extremely weak mass signal even though it is an electronically stable dianion. Thus, the smallest cluster that we were able to obtain good quality data was the $n = 4$ species. Figure 2 shows the PES spectra of $SO_4^{2-}(H_2O)_n$ that we obtained at 355 nm. Despite the low electron binding energies of the small clusters, we were only able to observe PES features for the $n = 4$ and 5 species because of the RCB. As we will show later, the 355 nm photon energy was likely below the RCB even for the $n = 4$ and 5 species and the relatively weak PES signals observed were actually due to electron tunneling.[56]

3.3. PES at 266 nm. The PES spectra at 266 nm are given in Figure 3. At this photon energy, we were able to obtain PES signals up to $n = 8$. The signals for the spectrum of $SO_4^{2-}(H_2O)_8$ were very weak and they were in fact due to electron tunneling. In all the 266 spectra, only one PES band was observed and its binding energy systematically increased with n.

3.4. PES at 193 nm. The 193 nm spectra are shown in Figure 4. We reported the 193-nm data for $n = 4-10$ previously.[8] In the current study, we were able to obtain 193-nm spectra for n up to 18. Two additional high binding energy features were revealed at this photon energy, following a large energy gap. Throughout this size range, the PES spectra remain similar and their binding energies shift gradually to the higher side with each addition of a solvent molecule. The highest binding energy feature was very broad and was cut off by the RCB starting in the spectrum of $SO_4^{2-}(H_2O)_8$. Starting from $n = 10$, the second band was also cut off by the RCB and it completely disappeared beyond the spectra of $n = 14$. Finally, the PES signals began to decrease even for the first band for the large clusters and no signals could be observed beyond $n = 18$ at 193 nm.

3.5. PES at 157 nm. The most complete data set was obtained at 157 nm. The PES spectra at this photon energy are shown in Figure 5 from $n = 4-40$. In the smaller size range, the 157 nm spectra are similar to those at 193 nm without any new spectral features. However, as the solvent number increased above $n \approx 12$, three gradual changes were observed in the 157-nm spectra. First, the relative intensity of the low binding energy feature from SO_4^{2-} seemed to decrease and almost disappeared in the

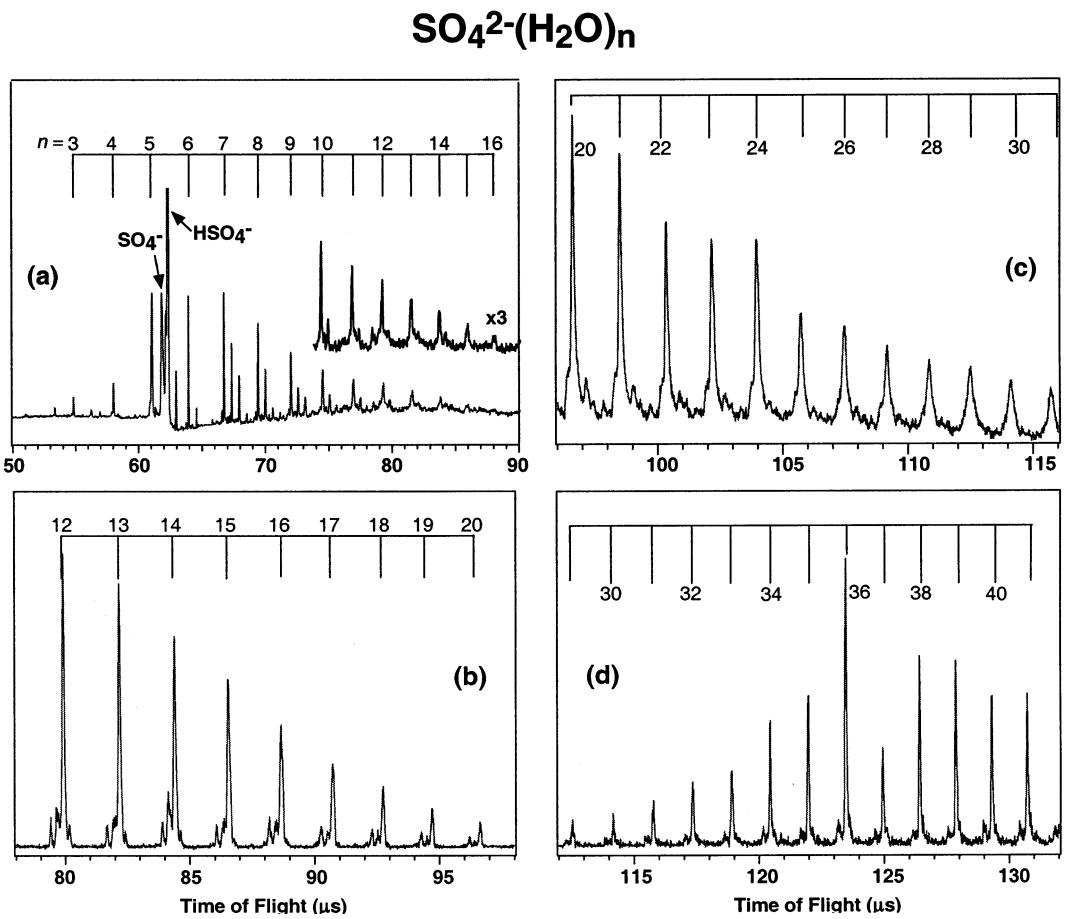

Figure 1. Typical mass spectra of $SO_4^{2-}(H_2O)_n$ using electrospray of a tetra-butylammonium sulfate solution and optimized for different cluster size ranges. (a) $n = 3-16$, (b) $n = 12-20$, (c) $n = 20-31$, and (d) $n = 31-41$. Note the general monotonic decrease of ion intensity as a function of size and the intense peak of $n = 36$.

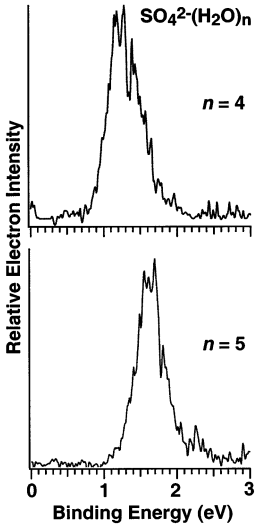

Figure 2. Photoelectron spectra of $SO_4^{2-}(H_2O)_n$ ($n = 4$ and 5) at 355 nm (3.496 eV).

large clusters ($n = 30$). Second, a very intense peak emerged at the high binding energy side, whereas no such bands were observed in the 193-nm spectra. Third, above $n \approx 12$, the gap between the first two bands became smaller, whereas it remained constant in the small clusters.

3.6. Adiabatic Detachment Energies (ADEs). The electronic stability of $SO_4^{2-}(H_2O)_n$, measured from the ADE of the lowest binding energy bands, increases steadily with the number of water, from ~0.4 eV ($n = 3$) to ~5.7 eV ($n = 40$). The ADE

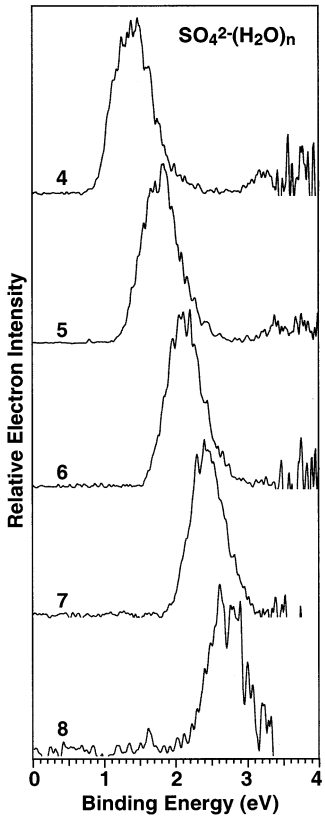

Figure 3. Photoelectron spectra of $SO_4^{2-}(H_2O)_n$ ($n = 4-8$) at 266 nm (4.661 eV).

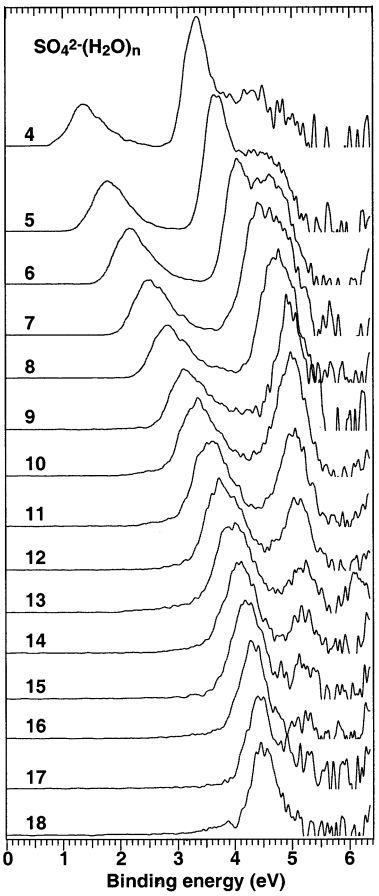

Figure 4. Photoelectron spectra of $SO_4^{2-}(H_2O)_n$ ($n = 4-18$) at 193 nm (6.424 eV).

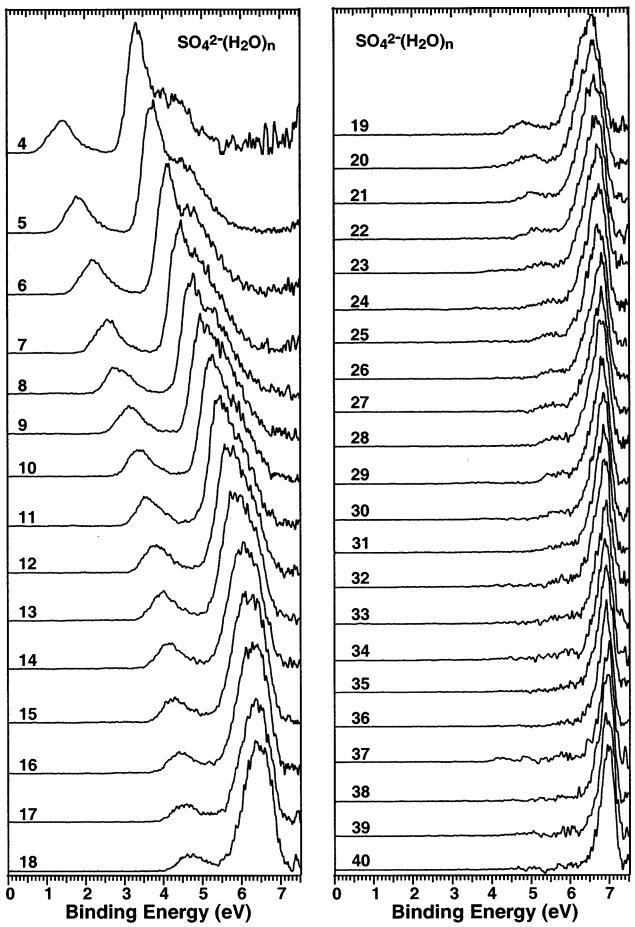

Figure 5. Photoelectron spectra of $SO_4^{2-}(H_2O)_n$ ($n = 4-40$) at 157 nm (7.866 eV).

for the smallest stable cluster, $SO_4^{2-}(H_2O)_3$, was estimated from a very weak detachment band obtained at 355 nm, as reported previously.[8] The broadness of the first feature made it difficult to determine the ADEs accurately, particularly for the large clusters of $n > 30$, where the first PES feature almost completely disappeared. The ADEs were estimated by drawing a straight line at the leading edge of the relevant photodetachment band and adding the instrumental resolution to the intersection with the binding energy axis. This procedure, though rather approximate, yielded relatively accurate and consistent ADEs for the smaller clusters, where the first PES band was well resolved. However, for larger clusters beyond $n = 30$, the uncertainties of the obtained ADEs were relatively large because of the very weak PES band. The obtained ADEs were given in Table 1 and plotted in Figure 6 as a function of n.

4. Discussion

4.1. Nature of the PES Features of $SO_4^{2-}(H_2O)_n$: Comparison to $Na^+(SO_4^{2-})$. The spectral shift of $SO_4^{2-}(H_2O)_n$ as a function of solvent number is rather rigid, i.e., all the spectra of the small clusters are very similar. Interestingly, the PES features of $SO_4^{2-}(H_2O)_n$ are nearly identical to those of $Na^+(SO_4^{2-})$,[50] indicating that the SO_4^{2-} dianion is responsible for the PES features and that it remained intact in the solvated clusters.

Figure 7 compares the 157-nm spectra of $SO_4^{2-}(H_2O)_n$ ($n =$ 4 to 6) and $Na^+(SO_4^{2-})$. The spectrum of the latter is well understood.[50] The lowest binding energy peak (X') at ~2 eV in the spectrum of $Na^+(SO_4^{2-})$ (Figure 7d) was due to the ion-pair dimer dianion, $[Na^+(SO_4^{2-})]_2$, which has identical m/z as the monomer, $Na^+(SO_4^{2-})$. The intensity of the dimer and, hence, the intensity of the X' peak could be minimized by changing the ESI source conditions, but could not be completely eliminated. We have previously shown that the second band of the $[Na^+(SO_4^{2-})]_2$ dimer had about the same binding energy as the first band of the monomer.[50] Therefore, the intensity of the first band of $Na^+(SO_4^{2-})$ (the X feature in Figure 7d) contained contributions from the second band of the dimer. As we showed previously, the three detachment features of the ion-pair can be understood by considering the valence molecular orbitals (MOs) of T_d SO_4^{2-}. The highest occupied MO (HOMO) of SO_4^{2-} is the triplet degenerate t_1 orbital and the MO below the HOMO (HOMO-1) is another triplet degenerate MO, t_2.[51] Electron detachments from these two MOs are responsible for the observed PES features of $Na^+(SO_4^{2-})$. Under the reduced symmetry (C_{3v}) of $Na^+(SO_4^{2-})$, the two degenerate MOs of SO_4^{2-} will be split. However, the splitting of the t_1 HOMO is too small to be resolved and it corresponds to the X band in the PES spectrum. The splitting of the t_2 MO is large enough, resulting in the A and B bands in the PES spectrum (Figure 7d).[50]

The PES features of the $SO_4^{2-}(H_2O)_n$ solvated species can be interpreted similarly.[8] The spectra of the solvated species are slightly broader, probably due to the reduced symmetry and the cluster temperatures. But the observed features and their relative positions are identical. The separation between the X and A bands is 2 eV and it remains the same in the spectra of the smaller solvated clusters independent of the solvent number. The relatively high intensity of the X band in the spectrum of the ion-pair was due to the contributions from the dimer, as

TABLE 1: Adiabatic Electron Detachment Energies (ADE) of SO_4^{2-} and Threshold Ionization Potentials (IP) of Water in Hydrated $SO_4^{2-}(H_2O)_n$ Clusters (n = 3-40)[a]

n	ADE (eV)	IP(eV)
3	0.4 ± 0.1	
4	0.92 ± 0.08	
5	1.36 ± 0.08	
6	1.71 ± 0.08	
7	2.08 ± 0.08	
8	2.38 ± 0.08	
9	2.68 ± 0.08	
10	2.96 ± 0.08	
11	3.16 ± 0.08	
12	3.34 ± 0.08	
13	3.51 ± 0.08	
14	3.66 ± 0.08	5.44 ± 0.10
15	3.84 ± 0.08	5.53 ± 0.10
16	3.96 ± 0.08	5.63 ± 0.10
17	4.07 ± 0.10	5.73 ± 0.10
18	4.22 ± 0.10	5.82 ± 0.10
19	4.35 ± 0.10	5.89 ± 0.10
20	4.43 ± 0.10	5.97 ± 0.10
21	4.64 ± 0.10	6.03 ± 0.10
22	4.70 ± 0.10	6.08 ± 0.10
23	4.76 ± 0.10	6.15 ± 0.10
24	4.97 ± 0.10	6.21 ± 0.10
25	5.11 ± 0.10	6.25 ± 0.10
26	5.19 ± 0.10	6.26 ± 0.10
27	5.15 ± 0.10	6.32 ± 0.10
28	5.20 ± 0.10	6.28 ± 0.10
29	5.22 ± 0.10	6.37 ± 0.10
30	5.22 ± 0.15	6.40 ± 0.10
31	5.32 ± 0.15	6.42 ± 0.10
32	5.42 ± 0.15	6.47 ± 0.10
33	5.43 ± 0.15	6.51 ± 0.10
34	5.48 ± 0.15	6.50 ± 0.10
35	5.65 ± 0.15	6.51 ± 0.10
36	5.66 ± 0.15	6.58 ± 0.10
37	5.60 ± 0.15	6.61 ± 0.10
38	5.70 ± 0.15	6.59 ± 0.10
39	5.73 ± 0.15	6.60 ± 0.10
40	5.73 ± 0.15	6.61 ± 0.10

[a] The ADEs for n = 3−5 were measured from the 355 nm spectra, those for n = 6−8 from the 266 nm spectra, and those for n = 9−18 from the 193 nm spectra. The ADEs for n >18 and all IP data were from the 157 nm spectra.

mentioned above. However, the *B* band of the solvated clusters appeared to be quite different. It was much broader and had much higher intensity, which appeared to increase in the large clusters. As we will discuss below, the *B* feature of $SO_4^{2-}(H_2O)_n$ (n = 4 to 6) contained considerable contributions from ionization of the solvent water molecules, which would eventually dominate the PES spectra of the large systems.

4.2. Spectral Evolution with Size and the Centrally Solvated SO_4^{2-} Dianion. The most surprising observation is the apparently gradual decrease of the first PES band of the SO_4^{2-} features and the increase of the second band with increasing solvation in the 157-nm spectra (Figure 5). The ratio of the first to the second band, measured from the 157-nm spectra, began to decrease significantly from n = 13, as shown in Figure 8. In fact, we noted that the photoelectron yield or detachment cross section in the 193 nm spectra, also plotted in Figure 8, also decrease from n = 13, when normalized to the ion intensity and photon flux. More surprisingly, the SO_4^{2-} features almost completely disappeared and the high binding energy peak became the dominant feature in the spectra of the large clusters (n > 30).

The PES spectra presented in Figures 2−5 represent transitions from the doubly charged solvated clusters to singly charged species. The spectral changes observed in the large solvated

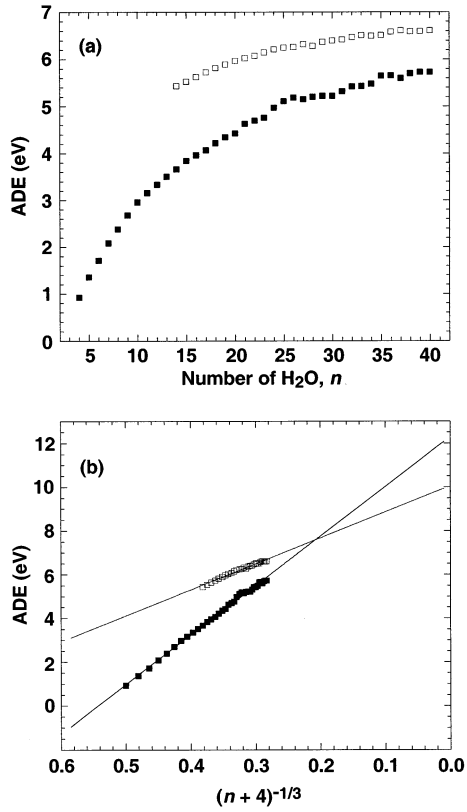

Figure 6. (a) Adiabatic detachment energies (ADE) of SO_4^{2-} (solid squares) and ionization thresholds of H_2O (open squares) in $SO_4^{2-}(H_2O)_n$ as a function of solvent number (n). (b) ADE of SO_4^{2-} (solid squares) and ionization thresholds of H_2O (open squares) in $SO_4^{2-}(H_2O)_n$ as a function of $(n+4)^{-1/3}$ (proportional to 1/cluster-radius).

clusters were not anticipated because, as the solvent number increased, the solutes were expected to remain intact. In particular, the loss of the solute PES features in the large clusters was a total surprise. Chemical changes, such as intra-cluster proton transfer, could be ruled out because the large solvated clusters represented more "diluted solutions," and the chemical equilibrium should favor the intact dianions as solvent number increased. In the only previous PES studies of large hydrated anions, i.e., $I^-(H_2O)_n$, PES features from the solute I^- were observed for n as large as 60.[32] PES of the hydrated electron also showed strong emission for up to 69 water molecules.[57] Interestingly, the I^- anion has since been known to be on the surface of the water clusters.[36,38,39] The disappearance of the solute signals in the large $SO_4^{2-}(H_2O)_n$ clusters suggested that the SO_4^{2-} dianion might be solvated in the center of the water clusters such that photoelectrons from the centrally located solute might not readily escape the increasing solvent layers. This difference between SO_4^{2-} and I^- could arise from the stronger charge-dipole interactions between the dianion and the water compared to the single diffuse charge of I^-. Previous ab initio calculations for up to six waters showed that indeed the water molecules tend to solvate symmetrically around SO_4^{2-}.[8]

This interpretation is supported by a previous PES study at 21.2 eV of a highly concentrated aqueous solution of CsF.[58] In this experiment, PES from F^- were significantly reduced by a one-layer water solvation shell on F^- at the solution-vacuum interface.[59] Furthermore, a small mixture of CsI into the CsF solution showed that PES features from I^- were actually enhanced because I^- was more surface-active. These observations in the bulk electrolyte solutions were consistent with the observations in the gas-phase solvated clusters, where I^- is

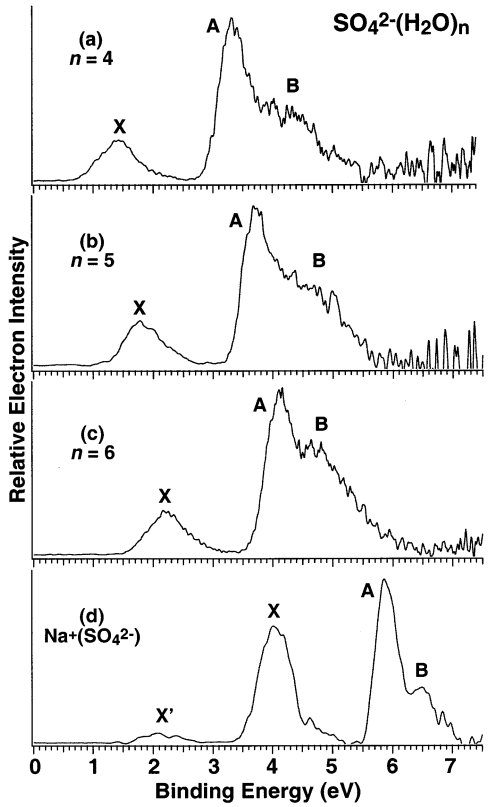

Figure 7. Comparison of the 157-nm spectra of $SO_4^{2-}(H_2O)_n$ (n = 4−6) to that of $Na^+(SO_4^{2-})$.

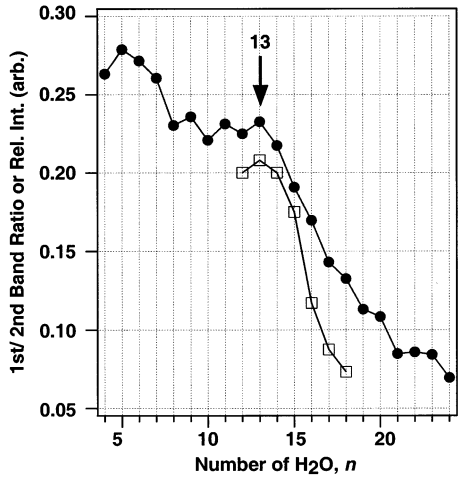

Figure 8. Ratio of the relative intensities of the first to the second PES band at 157 nm (solid circles) and the normalized relative intensity of the first PES band at 193 nm (open squares) as a function of number of water.

known to be solvated on the outside of the water clusters[36,38,39] and F^- on the inside due to its strong charge-dipole interactions with water.[34,39]

4.3. Spectral Evolution with Size and the Appearance of Ionization Feature from the Solvent. As pointed out earlier, the spectral shift in the small $SO_4^{2-}(H_2O)_n$ clusters are rigid, because the SO_4^{2-} dianion remains intact and the same in each cluster. However, for $n > 13$, the first band clearly began to decrease. At the same time, the separation between the first two bands also appeared to become smaller. If we assume that the SO_4^{2-} features were to remain the same in all clusters, the above observations suggested that there might be a new feature growing in as a function of cluster size and contributing to the second band of the SO_4^{2-} PES features. Eventually, this new feature became the dominant one in the PES spectra of the large clusters, as the SO_4^{2-} signals began to diminish.

What is the nature of this high binding energy feature? Inelastic scatterings[60] of photoelectrons from the centrally solvated SO_4^{2-} by the water layer can be ruled out as the major contributor for two reasons. First, this new feature is too intense and the signals seemed to increase with the number of solvent molecules, despite the fact that the mass signals of the large clusters gradually decreased. Second, this band did not exist in the 193-nm spectra (Figure 4). If it were due to inelastic scatterings, it would be expected to exist in the 193-nm spectra for $n > 13$. Therefore, the high binding energy feature must be due to a new detachment channel that gained cross section with cluster size and cannot be accessed at 193 nm. This new detachment channel was attributed to ionization of water. The ionization potential of water clusters should be between that of gaseous water molecules at 12.6 eV and that of liquid water at 10.06 eV.[61] Because our solvated clusters were negatively charged, the ionization potentials of water should be lowered. In fact, we recently observed that the ionization potential of a water molecule was reduced from 12.6 eV to about 6.1 eV in the F^-H_2O complex, because of the strong Coulomb repulsion experienced by the valence electrons in H_2O from F^-.[62]

In fact, we suspected that the *B* band in the PES spectra of the smaller $SO_4^{2-}(H_2O)_n$ clusters, which was broad and intense when compared to the corresponding feature in the spectrum of $Na^+(SO_4^{2-})$ (Figure 7), already contained contributions from the ionization of water. This was confirmed by preliminary MO calculations,[63] which showed that for $SO_4^{2-}(H_2O)_4$ the MOs derived from waters closely followed the t_2 MOs of the SO_4^{2-}. Because of the overlap between the solvent ionization feature and those due to the solute, we could not definitively determine the solvent ionization potentials in the smaller clusters. However, as the cluster size increased, the cross section of the solvent ionization increased. And at the same time, its relative ionization potential decreased, such that it began to overlap with the *A* band of the solute features. We suspected that the relative intensity change between the first two solute bands starting around $n = 13$ was due to contributions of the water ionization feature to the second solute band. Furthermore, the closing separation between the first and second bands starting in the same size range suggested that the binding energy for the ionization of water was actually smaller than that of the second solute band. Therefore, the threshold of the second band at large n actually represented the ionization threshold of water for $n >$ 13. Our estimated solvent ionization thresholds, determined from the second PES band, are also given in Table 1 and plotted in Figure 6 as a function of solvent number.

Previous theoretical considerations of ion solvation in finite clusters suggested that the ionization energies of a solvated anion should be scaled to $1/R$ linearly,[64,65] where R is the radius of the solvated clusters and is proportional to the solvent number as $(n + \delta)^{-1/3}$ (δ is the equivalent solvent number for the solute and accounts for the contribution of the solute to the cluster volume[66]). For example, in $I^-(H_2O)_n$, δ has been taken to be 2 for I^-.[32] We estimated that δ is 4 for SO_4^{2-}. In Figure 6, we also plotted the ionization thresholds for the solutes and solvent as a function of $(n+\delta)^{-1/3}$. The ionization thresholds for the solutes as well as that for water were indeed linearly dependent on $(n + \delta)^{-1/3}$. Importantly, the ionization energies for water extrapolated to 10.05 eV, for infinitive n, and are consistent with the threshold ionization energy of bulk water at 10.06 eV.[61] This observation lent considerable credence for the assignment

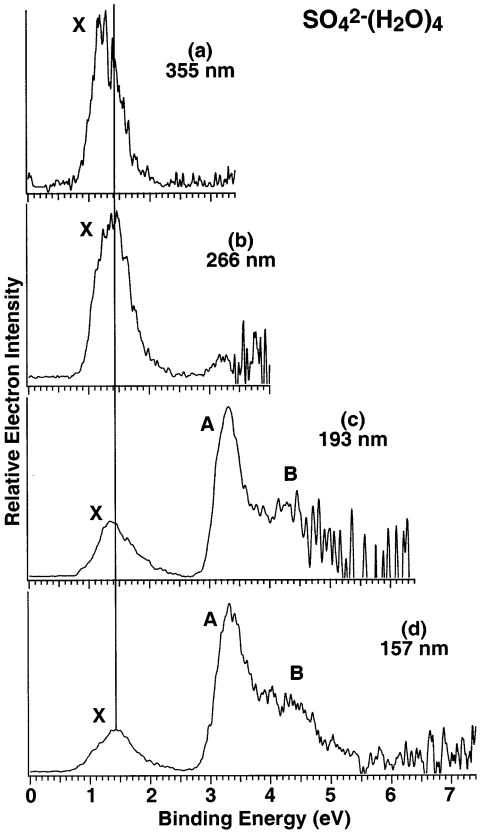

Figure 9. Photoelectron spectra of $SO_4^{2-}(H_2O)_4$ at (a) 355, (b) 266, (c) 193, and (d) 157 nm.

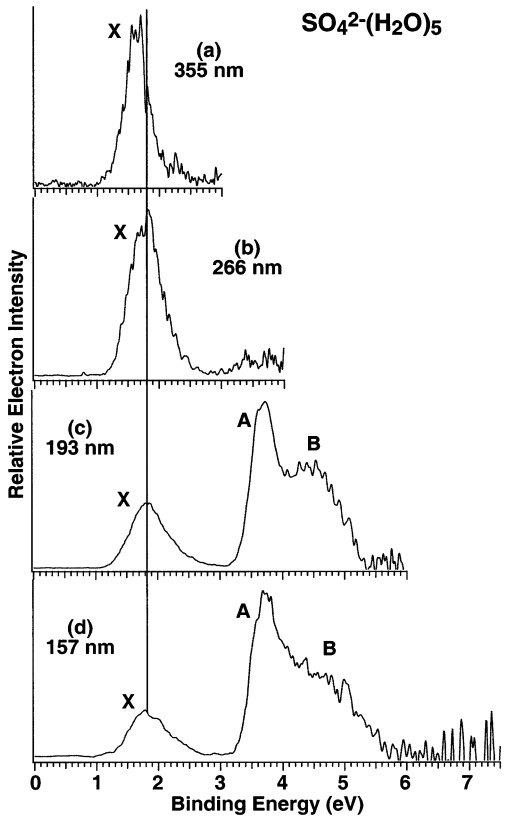

Figure 10. Photoelectron spectra of $SO_4^{2-}(H_2O)_5$ at (a) 355, (b) 266, (c) 193, and (d) 157 nm.

of the high binding energy feature to ionization of water in the solvated systems. The ionization energies of the solute extrapolated to a very large value, 12.3 eV for $SO_4^{2-}(H_2O)_n$ for infinitely large clusters. In bulk aqueous solutions, the threshold ionization energy of SO_4^{2-} was measured to be 8.65 eV.[61] We attributed this discrepancy to the fact that the bulk value was measured over the surface of aqueous solutions at relatively high solute concentrations, whereas our extrapolations corresponded to a hypothetical situation in which a single solute is solvated in the center of an infinitely large water cluster (i.e., an infinitely dilute solution).

4.4. Photon Energy Dependent Studies and the Repulsive Coulomb Barriers (RCBs). One unique property of MCAs is the existence of the intramolecular Coulomb repulsion between the excess charges. When an electron is removed from an MCA (AB^{n-}), the two photoproducts ($AB^{(n-1)-} + e^-$) are both negatively charged. The superposition of the long-range Coulomb repulsion between the outgoing electron and the remaining anion and the short-range electron binding produces an effective potential barrier for the outgoing electron.[6,53−56] If the detachment photon energy is below the top of the RCB, no electron detachment will occur even if the photon energy is above the asymptotic electron binding energy. In this case, detachment can only take place through electron tunneling, which depends exponentially on the distance between the photon energy and the RCB top and become negligible if the photon energy is far below the barrier top. When the photon energy is around the RCB top, the detachment signal may be reduced. In the tunneling regime, the appearance of the PES peak tends to shift to the lower binding energy side, due to a convolution of Franck−Condon factors and tunneling probabilities,[56] which depend on the electron kinetic energies exponentially. The intramolecular Coulomb repulsion and the resulting RCB have profound effects on the chemical and physical properties of MCAs. We have shown that the Coulomb repulsion is equal in magnitude to the RCB if the detached electron corresponds to the negative charge carrier or is localized on the charge carrier group.[55,67] In general, the RCB decreases with increasing physical sizes for MCAs.

We have measured photon-energy-dependent PES spectra of $SO_4^{2-}(H_2O)_n$ for $n = 4-18$. For $SO_4^{2-}(H_2O)_4$ and $SO_4^{2-}(H_2O)_5$, we were able to obtain their PES spectra at all four photon energies, as compared in Figures 9 and 10, respectively. There were no detectable electron signals at 355 nm for $n > 6$. At 266 nm, we were only able to obtain data for up to $n = 8$ (Figure 3) and at 193 nm for up to $n = 18$ (Figure 4). We can estimate the magnitudes of the RCB from these photon-energy-dependent data. Here, we use the spectra of $SO_4^{2-}(H_2O)_4$ as an example (Figure 9). Note that vertical detachment energies (VDEs) are used in estimating the RCB. The disappearance of feature *A* in the 266-nm spectrum indicates that the 266-nm photon energy lies below the top of the RCB corresponding to this channel. Thus, the RCB has to be larger than 1.2 eV ($h\upsilon$ - VDE of the *A* state, i.e., 4.6−3.4). The strong *X* peak (VDE = 1.4 eV) in the 266-nm spectrum implies that the 266-nm photon energy is above the RCB of the *X* state. Thus, the RCB should be smaller than 3.2 eV (4.6 − 1.4 eV). At 355 nm, only the first feature (*X*) was observed, but it appeared to be shifted to the low binding energy side. The shift was due to the electron tunneling effect,[56] indicating that the 355 nm photon energy was below the RCB of the *X* state. This suggested that the RCB should be larger than 2.1 eV (3.5 eV− 1.4 eV). So we obtained the RCB to be in the range of 2.1 to 3.2 eV for $SO_4^{2-}(H_2O)_4$. Similarly, we estimated the RCB for $SO_4^{2-}(H_2O)_5$ from the photon-energy-dependent PES spectra in Figure 10 to be in the range of 1.7 to 2.8 eV. We were able to obtain upper and lower bounds for the RCB for detaching an electron from SO_4^{2-} in $SO_4^{2-}(H_2O)_n$ for

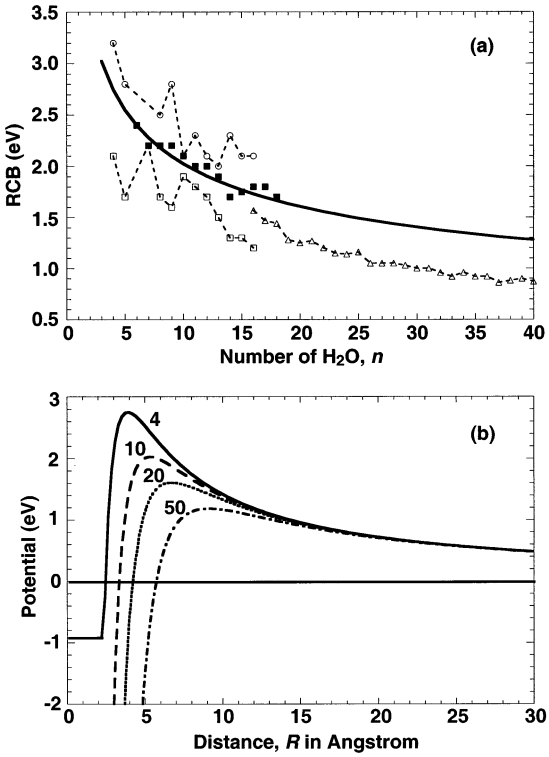

Figure 11. (a) Experimentally estimated RCBs for detachment from SO_4^{2-} (open circles—upper bounds, open squares—lower bounds, solid squares—most probable values obtained when photon energies were near RCB tops. See Text.) and for ionization of water (open triangles) as a function of solvent number (n). The solid curve is from a model calculation of the RCB for electron detachment from SO_4^{2-} (See Figure 12). (b) Calculated RCBs as a function of separation between the outgoing electron and the remaining singly charged $SO_4^-(H_2O)_n$ anion for $n = 4$, 10, 20, and 50. The well depths correspond to the ADE of each cluster (Table 1).

n up to 18. These data (upper and lower bounds) were plotted in Figure 11 as open circles and open squares. For $SO_4^{2-}(H_2O)_6$, its first PES band at 266 nm (Figure 3) was observed to be strong, but slightly shifted to the lower binding energy side relative to that in the 193-nm spectrum, suggesting that the 266-nm photon energy was around the RCB top of the X band. Thus, we obtained the most probable RCB to be ~2.4 eV [(4.6 − 2.2 eV (the VDE of the X band)]. In such cases when the photon energy happened to be near a barrier top, the most probable RCB so obtained is more accurate than the bracketing procedure can yield. These most probable RCBs obtained for certain cluster sizes of $SO_4^{2-}(H_2O)_n$ are plotted in Figure 11 as solid squares.

The estimated RCBs for the solvated SO_4^{2-} dianions decrease with increasing solvent numbers from ~2.8 eV for $n = 4$ to ~1.7 eV for $n = 18$. These results indicate that the intramolecular Coulomb repulsion within the solvated SO_4^{2-} clusters decrease as a function of cluster size and represent a dramatic reduction compared to that of bare SO_4^{2-}, which is so high as to rendering it electronically unstable.[51] The S−O bond length in bare SO_4^{2-} was calculated to be 1.52 Å,[8] which is very close to the corresponding values of 1.47−1.50 Å in various crystals, 1.50 Å in molten salts and solutions.[51] If we use a point charge model and assume that the charges were localized on two O atoms, we would evaluate a Coulomb repulsion of ~5.8 eV in isolated SO_4^{2-} using an O−O distance of 2.5 Å, which is consistent with a recent resonance structure calculation.[52] Such a large intramolecular Coulomb repulsion makes SO_4^{2-} extremely unstable as an isolated dianion against spontaneous electron emission. In the solvated clusters, two factors contribute to the stabilization of the dianion or the reduction of the Coulomb repulsion: the strong H-bonds formed between the dianion and H_2O and the dielectric shielding effect of the solvent.

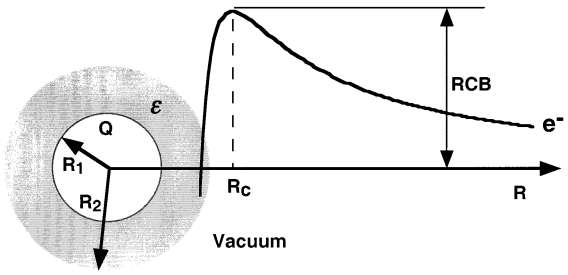

Figure 12. Electrostatic model used to calculate the RCB for detaching an electron from SO_4^{2-} in $SO_4^{2-}(H_2O)_n$. The $SO_4^-(H_2O)_n$ solvated clusters were modeled as a charged sphere (radius R_1) imbedded in a dielectric sphere (with radium R_2, dielectric constant ϵ).

4.5. Electrostatic Model of the RCB. The RCB can be alternatively viewed as the potential barrier between an incoming electron and the singly charged SO_4^- solvated in the center of a water cluster, which can be simply modeled as a water droplet doped by a SO_4^- sphere, as shown schematically in Figure 12. The potential energy of interaction between an electron and a charged sphere (radius R_1) imbedded in a dielectric sphere (with radium R_2, dielectric constant ϵ) (Figure 12) is largely governed by the long-range Coulomb repulsion and the polarization,[68] as

$$W = -\frac{A}{R^4} + \frac{B}{R} \quad (\text{when } R > R_2) \tag{1}$$

where $A = (14.4/2)\alpha$ in (eVÅ^4), $B = 14.4$ in eVÅ, α is the polarizability (Å^3), and R is the distance between the center of mass of the charged ball and the approaching electron (because the $R > R_2$, there is no ϵ term).

The critical distance R_c, i.e., the R value corresponding to the top of the RCB, is derived from the zero derivative of W with respect to R, $\partial W/\partial R = 0$

$$\frac{\partial W}{\partial R} = \frac{4A}{R^5} - \frac{B}{R^2} = 0 \tag{2}$$

which yields

$$R_c = \left(\frac{4A}{B}\right)^{1/3} \tag{3}$$

Substitute R_c into eq 1, we obtain

$$\text{RCB} = \frac{3B}{4}\left(\frac{B}{4A}\right)^{1/3} = \frac{3B}{4R_c} \tag{4}$$

The explicit expression of A or α in term of RCB is

$$A = \frac{B}{4}R_c^3 = \frac{B}{4}\left(\frac{3B}{4\text{RCB}}\right)^3 = \frac{27}{256}\cdot\frac{B^4}{\text{RCB}^3} = \frac{4534.96}{\text{RCB}^3} \tag{5}$$

$$\alpha = \frac{A}{7.2} = \frac{629.86}{\text{RCB}^3} \tag{6}$$

For $n = 6$, we know RCB = 2.4 eV, which yields $\alpha = 45.56$. If we assume α is linearly proportional to the number of water molecules, $\alpha = k\cdot n$, where n is the number of solvent water, we obtain $k = 7.59$, and $A = 7.2\alpha = 7.2\cdot k\cdot n = 54.648\cdot n$ using the RCB for $n = 6$. Thus, we have

$$\mathrm{RCB} = \left(\frac{629.86}{\alpha}\right)^{1/3} = \left(\frac{629.86}{k \cdot n}\right)^{1/3} = 4.362 \cdot n^{-1/3}, \quad (7)$$

$$R_c = \frac{3B}{4RCB} = \frac{3B}{4 \cdot 4.362 \cdot n^{-1/3}} = 2.4759 n^{1/3}. \quad (8)$$

$$W = -\frac{A}{R^4} + \frac{B}{R} = -\frac{54.648 \cdot n}{R^4} + \frac{14.4}{R} \quad (9)$$

The calculated RCBs as a function of n and R for different clusters according to eqs 7−9 were plotted in Figure 11. The agreement between the model and the experimentally determined RCBs is excellent, indicating that the simple model provides a reasonable description of the RCB and interactions between the departing electron and the remaining anion.

4.6. RCB for the Solvent Ionization Channel. The RCB in MCAs is created by the superimposition of the short-range electron binding and the long-range Coulomb repulsion between the outgoing electron and the remaining negatively charged particle with one less electron. The charge distribution on the remaining particle is expected to influence the barrier height.[67,69] Detachment of one electron from the SO_4^{2-} solute results in a singly charged SO_4^- solvated by neutral water molecules, whereas ionization of the solvent leaves the SO_4^{2-} dianion intact with a positive hole on the solvent layer. Therefore, the RCB corresponding to detachment of an electron from the SO_4^{2-} solute or from ionization of water is expected to be different.

As we have shown previously, the high binding energy feature of the 157-nm spectra (Figure 5) was dominated by the ionization of water. More PES features were expected at even higher binding energies to be derived from water. But they were cut off by the RCB. Therefore, the RCB for the water detachment channel could be approximately estimated from the cutoff at the high binding energy side. The RCB so obtained for the water ionization channel is also plotted in Figure 11 as open triangles. Indeed, we observed that the RCB for detachment from SO_4^{2-} is consistently higher than the RCB for the water ionization channel. The smaller RCB of the water ionization channel and the relatively weak dependence of the water ionization threshold on cluster size (as seen from the smaller slope in Figure 6b) were responsible for the dominant water photoemission signals observed in the 157-nm spectra of the large clusters.

5. Conclusions

We report an extensive photoelectron spectroscopic study of the hydrated sulfate dianions, $SO_4^{2-}(H_2O)_n$ ($n = 4-40$), at four photon energies, 355, 266, 193, and 157 nm. Lower photon energies only allowed smaller clusters to be studied, and only the 157 nm photon allowed the full cluster size range to be studied. PES spectra of the small clusters were similar and dominated by emission features from the solute dianion via comparison with PES spectra of an ion-pair, $Na^+(SO_4^{2-})$. As the cluster size increased beyond $n \approx 13$, we observed that the solute PES features began to decrease and a new feature due to ionization of the solvent emerged. For large clusters with $n >$ 30, the solute features almost completely disappeared. The photon energy dependent spectra allowed us to estimate the repulsive Coulomb barrier, or the intramolecular Coulomb repulsion with the solvated doubly charged anions. We observed that the RCB is significantly reduced in the solvated clusters relative to the bare SO_4^{2-} and it decreases as more solvent is added. A simple electrostatic model was used to evaluate the RCB and excellent agreement was observed with the experimentally derived RCB. The RCB for the solvent ionization channel, estimated from the spectral cutoff, was found to be smaller than the RCB for detachment from the solute SO_4^{2-}. The bulk ionization potentials of water and aqueous SO_4^{2-} were determined from the extrapolation of the cluster data to be 10.05 and 12.3 eV, respectively.

Acknowledgment. We gratefully acknowledge valuable discussions throughout this work with Drs. A. I. Boldyrev, S. D. Colson, J. P. Cowin, and J. B. Nicholas. This work was supported by The U.S. Department of Energy, Office of Basic Energy Sciences, Chemical Science Division, and partly by The Petroleum Research Fund, administered by the American Chemical Society. The work was performed at the W. R. Wiley Environmental Molecular Sciences Laboratory, a national scientific user facility sponsored by DOE's Office of Biological and Environmental Research and located at Pacific Northwest National Laboratory, operated for DOE by Battelle.

References and Notes

(1) Compton, R. N. Multiply Charged Negative Ions. In. *Negative Ions*; Esaulov, V., Ed.; Cambridge University Press: Cambridge, 1996.
(2) Kalcher, J.; Sax, A. F. *Chem. Rev.* **1994**, *94*, 2291.
(3) Scheller, M. K.; Compton, R. N.; Cederbaum, L. S. *Science* **1995**, *270*, 1160.
(4) Boldyrev, A. I.; Gutowski, M.; Simons, J. *Acc. Chem. Res*. **1996**, *29*, 497.
(5) Schroder, D.; Schwarz, H. *J. Phys. Chem*. A **1999**, *103*, 7385.
(6) Wang, L. S.; Wang, X. B. *J. Phys. Chem. A* **2000**, *104*, 1978.
(7) Ding, C. F.; Wang, X. B.; Wang, L. S. *J. Phys. Chem. A* **1998**, *102*, 8633.
(8) Wang, X. B.; Nicholas, J. B.; Wang, L. S. *J. Chem. Phys*. **2000**, *113*, 10 837.
(9) Wang, X. B.; Yang, X.; Nicholas, J. B.; Wang, L. S. *Science* **2001**, *294*, 1322.
(10) Marcus, Y. *Ion Solvation*; Wiley: New York, 1985.
(11) Pasquarello, A.; Petri, I.; Salmon, P. S.; Parisel, O.; Car, R.; Toth, E.; Powell, D. H.; Fischer, H. E.; Heim, L.; Merbach, A. E. *Science* **2001**, *291*, 856.
(12) Kropman, M. F.; Bakker, H. J. *Science* **2001**, *291*, 2118.
(13) Geissler, P. L.; Dellago, C.; Chandler, D.; Hutter, J.; Parrinello, M. *Science* **2001**, *291*, 2121.
(14) Dedonder-Lardeux, C.; Grégoire, G.; Jouvet, C.; Martrenchard, S.; Solgadi, D. *Chem. Rev*. **2000**, *100*, 4023.
(15) Peslherbe, G. H.; Ladanyi, B. M.; Hynes, J. T. *Chem. Phys*. **2000**, *258*, 201.
(16) Rudolph, W. W.; Pye, C. C. *J. Phys. Chem. A* **2001**, *104*, 1627.
(17) Jalilehvand, F.; Spångberg, D.; Lindquist-Reis, P.; Hermansson, K.; Persson, I.; Sandström, M. *J. Am. Chem. Soc*. **2001**, *123*, 431.
(18) Herman, G. J.; Neilson, G. W. *J. Mol. Liquids* **1990**, *46*, 165.
(19) Niedner-Schatteburg, G.; Bondybey, V. E. *Chem. Rev*. **2000**, *100*, 4059.
(20) Cabarcos, O. M.; Weinheimer, C. J.; Lisy, J. M. *J. Chem. Phys*. **2001**, *110*, 8429.
(21) Steel, E. A.; Merz, K. M., Jr.; Selinger, A.; Castleman, A. W., Jr. *J. Phys. Chem*. **1995**, *99*, 7829.
(22) Blades, A. T.; Jayaweera, P.; Ikonomou, M. G.; Kebarle, P. *J. Chem. Phys*. **1990**, *92*, 5900.
(23) Wright, R. R.; Walker, N. R.; Firth, S.; Stace, A. J. *J. Phys. Chem. A* **2001**, *105*, 54.
(24) Peschke, M.; Blades, A. T.; Kebarle, P. *J. Phys. Chem. A* **1998**, *102*, 9978.
(25) Thompson, C. J.; Husband, J.; Aguirre, F.; Metz, R. B. *J. Phys. Chem. A* **2000**, *104*, 8155.
(26) Spence, T. G.; Burns, T. D.; Posey, L. A. *J. Phys. Chem. A* **1997**, *101*, 139.
(27) Knipping, E. M.; Lakin, M. J.; Foster, K. L.; Jungwirth, P.; Tobias, D. J.; Gerber, R. B.; Dabdub, D.; Finlayson-Pitts, B. J. *Science* **2000**, *288*, 301.
(28) Benderskii, A. V.; Eisenthal, K. B. *J. Phys. Chem. B* **2001**, *105*, 6698.
(29) Clary, D. C.; Benoit, D. M.; Mourik, T. V. *Acc. Chem. Res*. **2000**, *33*, 441.
(30) Parsegian, V. A. *Nature* **1995**, *378*, 335.
(31) Balbuena, P. B.; Johnston, K. P.; Rossky, P. J. *J. Phys. Chem*. **1996**, *100*, 2705.

(32) Markovich, G.; Pollack, S.; Giniger, R.; Cheshnovsky, O. *J. Chem. Phys*. **1994**, *101*, 9344.
(33) Ayotte, P.; Weddle, G. H.; Johnson, M. A. *J. Chem. Phys*. **1999**, *110*, 7129.
(34) Cabarcos, O. M.; Weinheimer, C. J.; Lisy, J.; Xantheas, S. S. *J. Chem. Phys*. **1999**, *110*, 5.
(35) Lehr, L.; Zanni, M. T.; Frischkorn, C.; Weinkauf, R.; Neumark, D. M. *Science* **1999**, *284*, 635.
(36) Perera, L.; Berkowitz, M. L. *J. Chem. Phys*. **1994**, *100*, 3085.
(37) Rips, I.; Jortner, J. *J. Chem. Phys*. **1992**, *97*, 536.
(38) Dang, L. X.; Chang, T.-M. *J. Phys. Chem. B*, in press.
(39) Jungwirth, P.; Tobias, D. J. *J. Phys. Chem. B* **2001**, *105*, 10 468.
(40) Yarne, D. A.; Tuckerman, M. E.; Klein, M. L. *Chem. Phys*. **2000**, *258*, 163.
(41) Waterland, M. R.; Stockwell, D.; Kelley, A. M. *J. Chem. Phys*. **2001**, *114*, 6249.
(42) Weber, J. M.; Kelley, J. A.; Nielsen, S. B.; Ayotte, P.; Johnson, M. A. *Science* **2000**, *287*, 2461.
(43) Blades, A,; Kebarle, P. *J. Am. Chem. Soc*. **1994**, *116*, 10 761.
(44) Stefanovich, E. V.; Boldyrev, A. I.; Truong, T. N.; Simons, J. *J. Phys. Chem. B* **1998**, *102*, 4205.
(45) Cannon, W. R.; Pettitt, B. M.; McCammon J. A. *J. Phys. Chem*. **1994**, *98*, 6225.
(46) Ohtaki, H.; Radnai, T. *Chem. Rev*. **1993**, *93*, 1157.
(47) Wang, L. S.; Ding, C. F.; Wang, X. B.; Barlow, S. E. *Rev. Sci. Instrum*. **1999**, *70*, 1957.
(48) Lau, T. C.; Wang, J.; Siu, K. W. M.; Guevremont, R. *J. Chem. Soc. Chem. Commun*. **1994**, 1487.
(49) Khairallah, G.; Peel, J. B. *J. Phys. Chem*. A **1997**, *101*, 6770.
(50) Wang, X, B.; Ding, C. F.; Nicholas, J. B.; Dixon, D. A.; Wang, L. S. *J. Phys. Chem. A* **1999**, *103*, 3423.
(51) Boldyrev, A. I.; Simons, J. *J. Phys. Chem*. **1994**, *98*, 2298.
(52) Simons, J.; Skurski, P.; Barrios, R. *J. Am. Soc. Soc*. **2000**, *122*, 11 893.
(53) Wang, X. B.; Wang, L. S. *Nature* **1999**, *400*, 245.
(54) Wang X. B.; Ding, C. F.; Wang, L. S. *Phys. Rev. Lett*. **1998**, *81*, 3351.
(55) Wang, L. S.; Ding, C. F.; Wang, X. B.; Nicholas, J. B. *Phys. Rev. Lett*. **1998**, *81*, 2667.
(56) Wang X. B.; Ding, C. F.; Wang, L. S. *Chem. Phys. Lett*. **1999**, *307*, 391.
(57) Coe, J. V.; Lee, G. H.; Eaton, J. G.; Arnold, S. T.; Sarkas, H. W.; Bowen, K. H.; Ludewigt, C.; Haberland, H.; Worsnop, D. R. *J. Chem. Phys*. **1990**, *92*, 3980.
(58) Bohm, R.; Morgner, H.; Oberbrodhage, J.; Wulf, M. *Surf. Sci*. **1994**, *317*, 407.
(59) Dietter, J.; Morgner, H. *Chem. Phys*. **1997**, *220*, 261.
(60) Faubel, M.; Steiner, B.; Toennies, J. P. *J. Chem. Phys*. **1997**, *106*, 9013.
(61) Delahay, P. *Acc. Chem. Res*. **1982**, *15*, 40.
(62) Yang, X.; Wang, X. B.; Wang, L. S. *J. Chem. Phys*. **2001**, *115*, 2369.
(63) Boldyrev, A. I., private communication.
(64) Barnett, R. N.; Landman, U.; Cleveland, C. L.; Jortner, J. *Chem. Phys. Lett*. **1988**, *145*, 382.
(65) Makov, G.; Nitzan, A. *J. Phys. Chem*. **1994**, *98*, 3459.
(66) Coe, J. V.; Earhart, A. D.; Cohen, M. H.; Hoffman, G. J.; Sarkas, H. W.; Bowen, K. H. *J. Chem. Phys*. **1997**, *107*, 6023.
(67) Wang, X. B.; Nicholas, J. B.; Wang, L. S. *J. Chem. Phys*. **2000**, *113*, 653.
(68) Compton, R. N.; Tuinman, A, A,; Klots, C. E.; Pederson, M. R.; Patton, D. C. *Phys. Rev. Lett*. **1997**, *78*, 4367.
(69) Dreuw, A.; Cederbaum, L. S. *Phys. Rev. A* **2001**, *63*, 12 501.